

2D vs 3D clustering of the elliptic particulates: The correlation with the percolation thresholds

Asghar Aryanfar^{a, ID, *}, Mahmoud Yamani^b, William A. Goddard III^c

^a Boğaziçi University¹, Bebek, Istanbul, 34342, Turkey

^b American University of Beirut, Riad El-Solh, 1107, Lebanon

^c California Institute of Technology, Pasadena, CA, 91125, USA



ARTICLE INFO

Keywords:

Continuum percolation
Elliptic fillers
2D vs 3D analysis
Original density
Connected density
Elemental density

ABSTRACT

We develop a continuum percolation procedure for the aggregation of the elliptic fillers in the 2 and 3-dimensional media. Given random distributions for the locus and rotations of the elements with a specified original density p , each medium achieves chains of elements through overlapping to achieve a connection density of ρ . In this regard, typically 3D aggregation is more efficient than 2D due to the possibility of additional connectivity from the in/out (i.e. depth) directions. Hence, when increasing the number of fillers the 3D percolation system experiences an early increase in the connection density ρ , which typically occurs in the neighborhood of the percolation threshold p_c . We initially develop a new iterative method to compute the percolation threshold p_c in finite systems. Subsequently, we show that such early divergence between 2D-3D percolation systems is followed by a later convergence stage, as the number of fillers progressively increases. Consequently, we show, conceptually and computationally, that the maximum 2D-3D difference in the connections density $\Delta\rho_{max}$ correlates directly with the respective 2D-3D difference in the percolation thresholds Δp_c , where a large pool of computational samples were generated by varying the aspect ratio as well as the relative scale of the particles. The results and respective analyses could be useful for the design of binary composite membranes of a specified thickness (i.e. thin \rightarrow 2D, thick \rightarrow 3D) for achieving the desired homogenized physical property.

1. Introduction

Percolation theory has been developed and utilized in a wide range of disciplines [1] as a powerful tool, particularly when combined with the probabilistic methods [2] such as randomness in the generation, distributions, and connection pattern of particulates [3]. The versatility of percolating media spans from the trees [4,5] and lattices [6,7] to multidimensional continuous particles [8], allowing the emergence of highly connected clusters providing specific thresholds [9], which is a measure for criticality [10].

Application-wise, the percolation thresholding is used to explain the sudden transition in physical/chemical behavior during the transport in the porous media [11] and underground hydrodynamic flows [12], to predict the morphology and fracture of composite materials [13], reaction kinetics [14], and biological systems [15]. Meanwhile, the percolation across the connected elliptic-shaped particles can be used for the percolation estimating the homogenized electrical [16] and thermal [17] conductivity

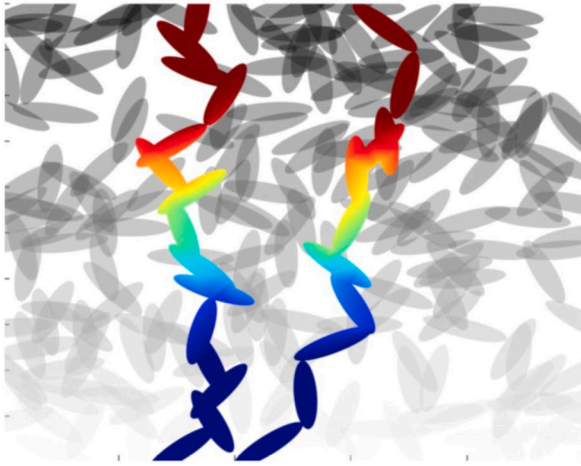
* Corresponding author at: Boğaziçi University, Bebek, Istanbul, 34342, Turkey.

E-mail address: aryanfar@caltech.edu (A. Aryanfar).

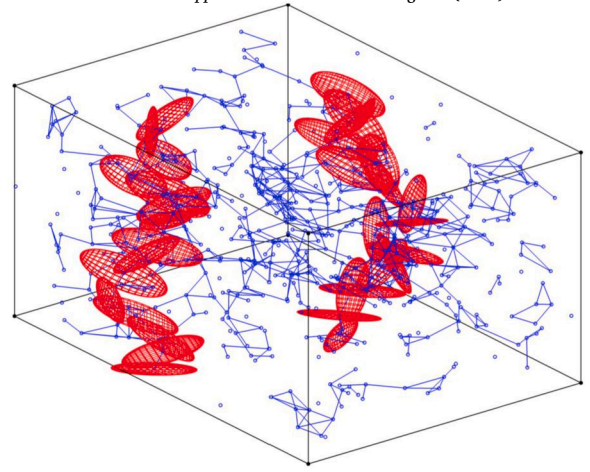
¹ a.k.a. Bosphorus University.

<https://doi.org/10.1016/j.apm.2025.116007>

Received 4 August 2024; Received in revised form 10 February 2025; Accepted 13 February 2025



(a) 2D percolation sample for edge-to-edge connection via the shortest path ($p_c = 0.64, \rho_0 = 0.004$) [16]. Gray ellipses: part of the original random distribution, colored ellipses: the connection pathways.



(b) 3D percolation sample for plane-to-plane connection via the shortest path ($p_c = 0.26, \rho_0 = 0.004$) [44]. Blue lines: the major axis for the ellipses of an original random distribution, red ellipses: the connection pathways.

Fig. 1. Examples of the enhancement in the top-to-bottom conductivity of the polymer medium (i.e. empty white space) via spreading the elliptic fillers of significantly higher conductivity in (a) 2 and (b) 3 dimensional domains, which is particularly achieved when connections are established [44].

of the binary composites, as well as the elastic modulus of fractures media [18], porous materials [19], which contain the excluded volume [20].

Mathematics-wise, several concepts have been developed to explain the percolation [21], such as the connection pattern of the adjacent elements [22], or the tight lower bound for the percolation threshold [23]. Materials-wise, the percolation has been utilized to study tensile modulus for polymer/clay nano-composites (PCN) [24], and the cementitious composites [25], the electrical conductivity of the resins [26] and composite polymers [27].

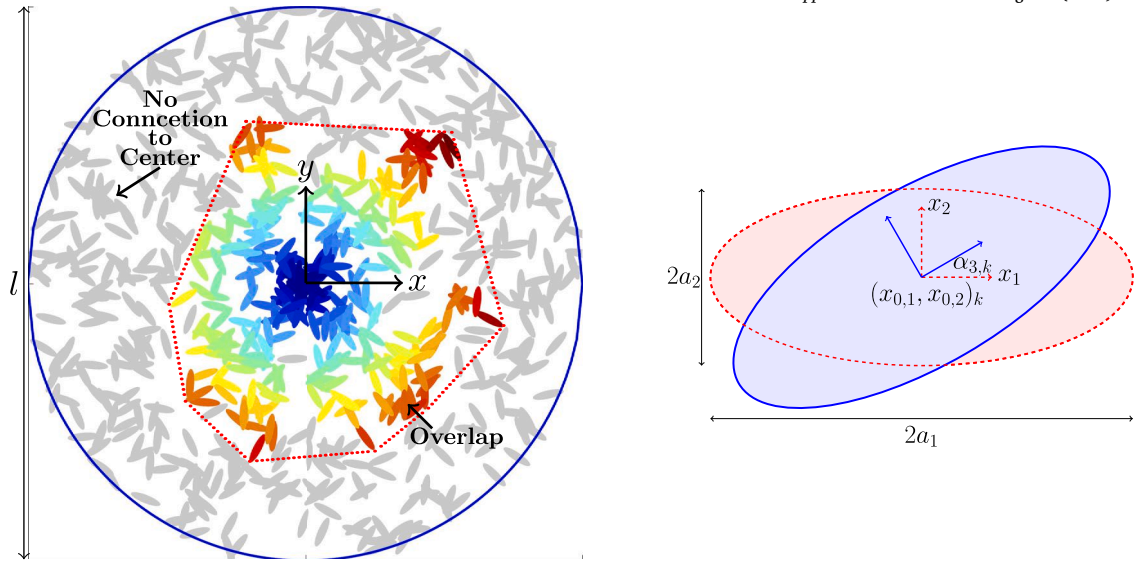
Meanwhile, the random placement of the specific shapes within continuous multidimensional domains has given rise to the formalization of continuum percolation theory [28]. In particular, micro-canonical simulations that use the union-find algorithms have been utilized, where accurate values for the percolation thresholds (i.e. density for end-to-end reach) have been found for several shapes such as squares [29], disks [30] rectangles [31], curved fibers (disco-rectangles) [32], concave-shaped (centrosymmetric) [33] and polydisperse [34] pores, where the combined role of pore shape and size determines the diffusivity [35] and permeability [36]. Additionally, the 2D versus 3D connection of elliptic particles has been compared with a focus on the medium-thickness [37].

Regarding the clustering behavior of the connected elements versus the original density p , several Sigmoidal (i.e. S-shape) models have been proposed, which illustrate the asymptotic converging trends both at initial and final connected density values ρ [38]. In this regard, the Sigmoidal-Boltzmann [39] and Sigmoidal-Dose [40] models provide similar results, the Sigmoid-Hill [41] and Sigmoid-Logistics [42] paradigms lead to diverging interpretations. In this regard, the shape approximation of the particles as elliptic geometry could be used as a tool for random geometries in the given granular medium [43].

In this paper, we develop both 2D and 3D models in circular (i.e. 2D) and spherical (i.e. 3D) domains for computing the center-initiated connected density ρ of the elliptic particulates, each with the elemental density of ρ_0 versus the given original medium density of p . In this regard, the connected density ρ of the propagating connected cluster, which is a measure for its maximum reach, is obtained and tracked for both 2D and 3D systems versus the elemental density ρ_0 of the filling particulates and their aspect ratio r . Subsequently, the maximum difference of the connected density $\Delta\rho_{max}$ in 2 and 3 dimensions has been found to be correlated with the difference in the center-to-border percolation thresholds (i.e. $\Delta p_c = p_{c,2} - p_{c,3}$). Consequently, the role of the shape of the ellipses/ellipsoids leading to the connected density ρ has been analytically addressed. The results and respective analyses could be used for determining the design of binary composite membranes of a specified thickness (i.e. thin \rightarrow 2D, thick \rightarrow 3D) to obtain the desired homogenized physical property, which is determined via the efficacy of the percolation.

2. Methodology

Given a dispersed medium of randomly placed elliptic particulates, there is a certain tendency for overlapping of the elements. Such tendency correlates directly with the original areal/volumetric density p as well as the geometry of the particles. For instance, Figs. 1a and 1b from prior works represent samples of the 2D and 3D edge-to-edge percolations via the connected elliptic elements, where the edge to edge connections are obtained in the original densities of $p_{c,2} \approx 0.64$ (2D) and $p_{c,3} \approx 0.26$ respectively (3D). Herein, we define the percolation procedure consisting of random placement of the elliptic/ellipsoidal particulates within a circular domain of the scale l , as shown in the Fig. 2a, where the dispersion of the ellipses/ellipsoids with original areal/volumetric density p has a certain tendency for making overlaps. Hence, beginning from the prescribed element in the center, some fraction of particulates could overlap and form a percolating cluster. The percolation procedure could stop, either when the connected cluster touches the



(a) The percolation model: The particles are randomly placed in a circular domain of scale l . The percolation starts from the central element and propagates via the overlappings toward the outer boundary (colored region) where the rest of the particles (gray) remain disconnected.

(b) Characterization of an ellipse indexed $k \in \{1, \dots, N\}$, with center position $x_{0,j}$ ($i \in \{1, 2\}$ in 2D and $i \in \{1, 2, 3\}$ in 3D), the axis a_i ($2a_1$ and $2a_2$ are shown), and the orientation α_j ($\alpha_{3,k}$ is shown; $j = 3$ in 2D and $j \in \{1, 2, 3\}$ in 3D).

Fig. 2. The percolation procedure: (a) the domain-scale characterization: The order of colors from blue to red commensurates with their distance from the central element. The convex hull of the propagating cluster is illustrated in a red dotted enclosure, which is a measure of the cluster reach. (b) the element-scale characterization.

boundary, or continue all the way, until no further progress can be made. The former determines the percolation threshold p_c , and the latter signifies the density of connected cluster ρ , as a fraction of the total. Hence:

$$\begin{cases} \text{Touching boundary} & \rightarrow \text{Percolation threshold } p_c \\ \text{All the overlaps considered} & \rightarrow \text{Connection Density } \rho \end{cases}$$

Since the connected cluster is a subset of original number of particulates, one has:

$$\rho \leq p \tag{1}$$

where the overlaps in the original density p and the connected density ρ are counted only once. In fact, if the original density p gets large enough, the cluster can reach the domain boundary, and the center-to-border connection gets established. The boundary is considered to be rigid, which means that the connection to the border does not transfer into the opposite direction (an event that occurs in periodic boundary condition). The original density leading to such center-to-end connection is the percolation threshold p_c .

Having one extra dimension, it is obvious that the continuum percolation in 3D has a higher possibility of making a connected cluster than its 2D counterpart,² and hence it will have an earlier end-to-end connection threshold occurring in a lower given original density p . As an example, a random distribution of the circular disks in a square domain achieves the end-to-end connection in the original density (i.e. percolation threshold) of $p_{c,2} \approx 0.68$ [30,45] while such connection occurs spherical elements randomly dispersed in a cubic domain, at very earlier original density $p_{c,3} \approx 0.29$ [46,47]. Therefore:

$$p_{c,3} \leq p_{c,2} \tag{2}$$

where $p_{c,2}$, $p_{c,3}$ are the percolation threshold of the 2 and 3 dimensions respectively, and the equal sign occurs when the third dimension becomes infinitely thin.

Such an early raise causes the connection density ρ to be higher in 3D than 2D counterpart in the same original density (i.e. when $p_3 = p_2$):

$$\rho_3 \geq \rho_2 \tag{3}$$

Considering the inequalities above Fig. 3, visualizes the anticipated growth pattern in the obtained connection density ρ versus the assigned original density p , as the particles fill the space progressively. Obviously, one could initially realize the following conditions, regardless of the dimension:

² The equivalency of the 2D and 3D systems will be addressed in the section 2.2.

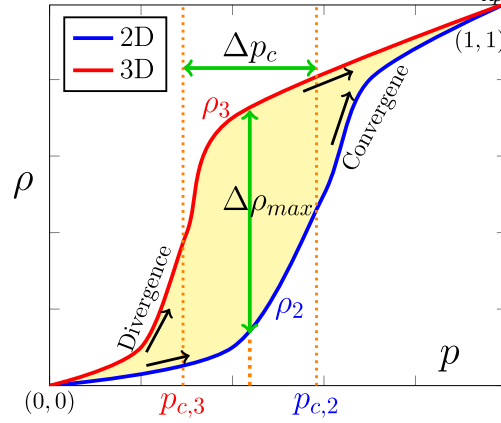


Fig. 3. The anticipated growth pattern in the connection density ρ versus the original density p , as the particles fill the space progressively in 2D (blue) and 3D (red) media. The span between early divergence (i.e. opening) and later convergence (i.e. closing) zones Δp_c , leads to a maximum difference in the connection density $\Delta \rho_{max}$.

- In the absence of any original ellipses in the medium ($p = 0$), no connecting cluster will exist ($\rho = 0$).
- When the particles fill the entire space ($p = 1$), all the particles become connected as well, and the connection density merges to unity ($\rho = 1$). In such a condition, the assigned number of particles N gets infinitely large ($N \rightarrow \infty$).

Thus for the relationship of original density versus connection density (p, ρ), the two initial and final positions of $(0,0)$ and $(1,1)$ will be shared between the 2D and 3D percolating systems. Nonetheless, since $\rho_3 \geq \rho_2$, the 3D percolation system will have an earlier increase, which forms the divergence zone as illustrated in the Fig. 3. However, since both percolation systems share the common final coordinate of $(1,1)$, such divergence, must be followed by a later convergence as shown in this Figure. Therefore a zone of difference is established between the two percolation systems, which roughly resembles a diamond. As well, the initial divergence and later convergence signifies the existence of a maximum difference value in the connection density $\Delta \rho_{max}$ occurring at a certain original density. In particular, since the significant portion of the increase in the density occurs at the percolation threshold value p_c , the span of the percolation thresholds in 2D and 3D (i.e. $[p_{c,3}, p_{c,2}]$) could be examined for exploring the location and the value of such maximum difference $\Delta \rho_{max}$. In fact, from the curves in Fig. 3, a larger difference in the percolation thresholds Δp_c would suggest a larger maximum difference in the connection density $\Delta \rho_{max}$. In other words, the larger width in the highlighted zone, should yield a correctable larger height as well, which we will computationally explore in detail.

2.1. Elliptic particulates

Fig. 2b illustrates the 2D sample of an elliptic particulate. Having the axial values a_i ($\{a_1, a_2\}$ in 2D and $\{a_1, a_2, a_3\}$ in 3D), center coordinates x_{0i} ($\{x_{01}, x_{02}\}$ in 2D and $\{x_{01}, x_{02}, x_{03}\}$ in 3D) and rotations α_i (α_3 in 2D and $\{\alpha_1, \alpha_2, \alpha_3\}$ in 3D), the loci of its surface x_i ($\{x_1, x_2\}$ in 2D and $\{x_1, x_2, x_3\}$ in 3D) can be defined as:

$$(X - X_0)^T R^T A R (X - X_0) = 1 \quad (4)$$

where X and X_0 are the locus of the border and center respectively as:

$$X = \begin{bmatrix} x_1 \\ x_2 \\ x_3 \end{bmatrix}, \quad X_0 = \begin{bmatrix} x_{01} \\ x_{02} \\ x_{03} \end{bmatrix} \quad (5)$$

and R is the rotation matrix around the 3 axis with values of α_1, α_2 and α_3 as:

$$R = \begin{bmatrix} 1 & 0 & 0 \\ 0 & \cos \alpha_1 & -\sin \alpha_1 \\ 0 & \sin \alpha_1 & \cos \alpha_1 \end{bmatrix} \begin{bmatrix} \cos \alpha_2 & 0 & \sin \alpha_2 \\ 0 & 1 & 0 \\ -\sin \alpha_2 & 0 & \cos \alpha_2 \end{bmatrix} \begin{bmatrix} \cos \alpha_3 & -\sin \alpha_3 & 0 \\ \sin \alpha_3 & \cos \alpha_3 & 0 \\ 0 & 0 & 1 \end{bmatrix} \quad (6)$$

The signs of the individual rotations in this model have been aligned and verified with the function *Sphere* in MATLAB, which is elaborated for individual rotations in Appendix B.

As well, the scaling matrix A is defined as:

$$A = \begin{bmatrix} \frac{1}{a_1^2} & 0 & 0 \\ 0 & \frac{1}{a_2^2} & 0 \\ 0 & 0 & \frac{1}{a_3^2} \end{bmatrix} \quad (7)$$

Table 1
The axis values for prolate and oblate ellipsoids as a function of aspect ratio r and the elemental density ρ_0 ($= \rho_{2,0} = \rho_{3,0}$).

Geometry	Prolate	Oblate
a_1	$\frac{\bar{a}}{\sqrt[3]{r^2}}$	$\frac{\bar{a}}{\sqrt[3]{r}}$
a_2	$\sqrt[3]{r\bar{a}}$	$\frac{\bar{a}}{\sqrt[3]{r}}$
a_3	$\sqrt[3]{r\bar{a}}$	$\sqrt[3]{r^2\bar{a}}$

In particular, the 2D procedure is a simplified version and can be established via removing the third dimension and assigning: $x_3 = x_{0,3} = 0$, $\alpha_1 = \alpha_2 = 0$, $a_3 = 1$. Similarly the notions of (< 1) and (> 1) represent if a point falls inside and outside the ellipse (ellipsoid) respectively. In this regard, the equivalency of the setup between the 2 and 3 dimensions has been defined as below:

2.2. Equivalent definitions

The geometrical characterization of the elliptical elements has been performed via normalizing the respective axis $a_1 \geq a_2 (\geq a_3)$ to a maximum (i.e. major) value a_1 , which forms the axial ratio r_i as:

$$r_i = \frac{a_i}{a_1} \tag{8}$$

Hence, the measure of the relative size of a single particle ρ_0 can be defined as:

$$\rho_0 = \frac{V_0}{V_{TOT}} \tag{9}$$

In this context, the 2D particle has been treated as a special case of a 3D ellipsoid, where the area A is a special form of volume V , as a measure for occupying space. V_0 is a volume (area) taken by a single particle and V_{TOT} is the total volume (area) for the circular domain of the scale l (in 2D: $V_{TOT} = \frac{\pi}{4}l^2$, and in 3D: $V_{TOT} = \frac{\pi}{6}l^3$). Meanwhile, $\rho_{2,0}$ and $\rho_{3,0}$ represent the elemental densities in 2 and 3 dimensions, respectively. Also, the original density p is simply defined as:

$$p = \frac{V}{V_{TOT}} \tag{10}$$

where V is the space occupied by the randomly dispersed original ellipses (excluding overlaps). Fig. 2a illustrates a 2D percolation sample, where the occupied space V accounts for all the connected ellipses to the central element (colored) and the unconnected ellipses (gray).

For the percolation, initiating from the central particle and growing through the overlapping particles, a cluster of connected elements is generated with the volume V_{clus} (excluding overlaps). Hence the obtained connected density ρ would be:

$$\rho = \frac{V_{clus}}{V_{TOT}} \tag{11}$$

The subscripts of 2, 3 in the Equations (10) and (11) (i.e. p_2, p_3 and ρ_2, ρ_3) denote the 2 or 3 dimensions respectively. The computing method for determining V and V_{clus} is explained later in the section 2.5.

The 2 and 3 dimensional procedures can be made equivalent by setting identical elemental densities ($\rho_{2,0} = \rho_{3,0}$). As well, the geometry is specified by ratios $(1, r_2)$ in 2D and by ratios $(1, r_2, r_3)$ in 3D. In order to avoid the third dimension as an extra degree of freedom, the geometry in 3D will be expressed in prolate $(1, r, r)$ and oblate $(1, 1, r)$ forms while that in 2D will be given by $(1, r)$.

The axis values a_i can be obtained directly from the elemental density ρ_0 and the aspect ratio r . In 2D, the elemental volume (area) is $V_0 = \rho_{2,0}V_{TOT}$, and the average radius \bar{a} would be $\bar{a} = \sqrt{\frac{V_0}{\pi}}$. Hence, the axis values a_1 and a_2 are obtained as:

$$a_1 = \frac{1}{\sqrt{r}}\bar{a}, a_2 = \sqrt{r}\bar{a} \tag{12}$$

Similarly, in 3D the elemental volume is $V_0 = \rho_{3,0}V_{TOT}$. The average radius \bar{a} becomes $\bar{a} = \sqrt[3]{\frac{3V_0}{4\pi}}$, for which the axis values a_1, a_2, a_3 for prolate and oblate geometries are obtained using Equation (8), as shown in Table 1.

Finally, by varying the elemental density ρ_0 and the axial ratio r , numerous percolation scenarios can be established in both 2D and 3D.

2.3. Adjacency matrix $\Gamma_{i,j}$

The connection of the percolating cluster is defined by the adjacency matrix $\Gamma_{i,j}$ which can be utilized to extract the percolation pathways. It is a boolean operator such that for elliptic particulates i and j :

$$\Gamma_{i,j} = \begin{cases} 1 & \text{Overlap} \\ 0 & \text{Separated} \end{cases} \quad (13)$$

and can be explored both analytically and numerically. In 2D, the surface equation (4) gets reduced to:

$$\begin{bmatrix} x_1 - x_{01} & x_2 - x_{02} \end{bmatrix} \begin{bmatrix} \cos \alpha_3 & \sin \alpha_3 \\ -\sin \alpha_3 & \cos \alpha_3 \end{bmatrix} \begin{bmatrix} \frac{1}{a_1^2} & 0 \\ 0 & \frac{1}{a_2^2} \end{bmatrix} \begin{bmatrix} \cos \alpha_3 & -\sin \alpha_3 \\ \sin \alpha_3 & \cos \alpha_3 \end{bmatrix} \begin{bmatrix} x_1 - x_{01} \\ x_2 - x_{02} \end{bmatrix} = 1 \quad (14)$$

where (x, y) is a location on the surface, (x_{01}, x_{02}) is the center coordinate, α_3 is the rotation angle normal to the plane, and a_1, a_2 are the major and minor axis respectively. A simple analytical mode for the overlap of two ellipses i and j is to use of the Vieillard-Baron contact function Ψ [48] as:

$$\Psi = 4(f_i^2 - 3f_j)(f_j^2 - 3f_i) - (9 - f_i f_j)^2$$

where the coefficients f_k ($k = \{i, j\}$ to avoid repetition) are the coefficients in the cubic polynomial of eigenvalues derived by setting the determinant of the pencil of conics of the intersection points between the two ellipses to zero, and Ψ is the discriminant of this determinant. The coefficients f_k are defined as: [49–51]:

$$f_k = 3 + A - B - C$$

and the coefficients A, B, C are obtained as:

$$A = \left(\frac{a_i}{a_j} - \frac{a_j}{a_i} \right)^2 \sin^2(\theta_j - \theta_i)$$

$$\begin{bmatrix} B \\ C \end{bmatrix} = \begin{bmatrix} \frac{1}{a_1} & 0 \\ 0 & \frac{1}{a_2} \end{bmatrix} \begin{bmatrix} \cos \theta_k & \sin \theta_k \\ -\sin \theta_k & \cos \theta_k \end{bmatrix} \begin{bmatrix} x_{01,2} - x_{01,1} \\ x_{02,2} - x_{02,1} \end{bmatrix}$$

The connection criterion is thus extracted from the sign of the discriminant and determinant coefficients as follows [48]:

$$\text{if } \{ \Psi < 0 \text{ or } \{ \Psi, f_1, f_2 \} > 0 \} \rightarrow \Gamma_{i,j} = 1$$

In 3D, previously several methods have been expressed for determining the overlap [52–54]. In this study we use the numerical method, in which we create a 3D grid in the entire domain and label the points falling inside each ellipsoid. In this regard, if two ellipsoids are too far apart, they are obviously separated. Therefore, to reduce the computational cost, one simple no-overlap condition is that the center-to-center distance should be greater than the sum of their largest axis a_1 :

$$\| \mathbf{X}_{0,i} - \mathbf{X}_{0,j} \| > 2a_1 \rightarrow \Gamma_{i,j} = 0 \quad (15)$$

Bypassing this condition, the intersection of the ellipses i and j requires sharing at least one identical inner point \mathbf{X} falling simultaneously in both volumes, satisfying the following condition:

$$\text{if } \exists X : \begin{cases} (X - X_{0,i})^T R_i^T A R_i (X - X_{0,i}) \leq 1 \\ (X - X_{0,j})^T R_j^T A R_j (X - X_{0,j}) \leq 1 \end{cases} \rightarrow \Gamma_{i,j} = 1 \quad (16)$$

where $X_{0,i}, X_{0,j}$ are the center positions and R_i, R_j are the rotation matrices of the ellipsoids i, j and A is the scaling matrix.

The accuracy of the adjacency matrix has been verified via multitudes of visualizations; examples are provided in the Appendix C.

2.4. Percolation threshold p_c

The percolation threshold p_c could be defined either as the minimum original density p where the propagating connected cluster achieves reach to the boundary of the circular medium, or the original density where 50% of the elements are part of the connected cluster. Herein we choose the former definition. The presented method for locating the percolation threshold p_c , is in fact an alternative description to the finite size scaling method (FSS) which is developed for finite systems (albeit we have explored a wide range of particle-to-domain scale). While the FSS method tracks the percolation probability p in various domain scales l , and estimates their overlaps as the threshold value p_c [55–57], this study considers only finite systems, where in addition to the particle geometry, the

relative scale of the particle to the domain ρ_0 ($\rho_0 = V_0/V_{TOT}$) is deterministic as well. In other words, observing from a broader perspective, obtaining a typical percolation threshold value p_c occurs for infinite systems and solely depends on the particle shape ($p_c = p_c(r)$), whereas this study operates on the finite systems, and in addition to the particle shape, its relative scale to the domain also becomes a deterministic factor ($p_c = p_c(r, \rho_0)$). Since the percolation threshold p_c depends on the elemental density ρ_0 and the axial ratio r , one could initialize from the largest possible range (i.e. $[0, 1]$). Hence:

$$0 \leq p_c \leq 1 \tag{17}$$

In order to estimate the percolation threshold p_c , we consecutively divide the given range to two halves, check the connection feasibility of the middle value and narrow-down by selecting the half containing the percolation threshold p_c , until reaching the required precision. Such threshold-containing interval should have no percolation at its minimum bound (denoted as 0) and percolation at its maximum bound (denoted as 1), so that the percolation threshold ($0 \rightarrow 1$) falls within this interval. In fact, the percolation threshold p_c is a margin separating two behavior regimes of no percolation (i.e. 0) and percolation (i.e. 1), and the selected interval should satisfy both behaviors in its minimum/maximum boundaries. For studying the percolation feasibility for the desired original density p , the original number of ellipses N can be spread over the circular domain and can be used as an initializing parameter. In the absence of overlaps (rare case scenario), the assigned original density p , directly correlates with the assigned original number of ellipses N , as below:

$$N \approx pN_{TOT} \tag{18}$$

where the approximation sign is used to round into the nearest integer and N_{TOT} is the total number of ellipses in ideal case that could cover the entire domain, with no overlaps, as:

$$N_{TOT} \approx \frac{V_{TOT}}{V_0} \tag{19}$$

However, the higher number of the objects N leads to the higher possibility of making overlaps and the rate of growth in the original density p slows down. In other words, the formation of the overlaps would require a larger number of original objects N for achieving a certain original density p , and one has:

$$N \geq pN_{TOT} \tag{20}$$

As a result, while there is no limit for the assigned objects N , the obtained original density p converges to the unity in the limit. Hence:

$$0 \leq N < \infty \Rightarrow 0 \leq p \leq 1 \tag{21}$$

Therefore, the algorithm for estimating the percolation threshold p_c gets established as follows:

0. In order to establish $0 \leq N < \infty$, initialize by assigning $[N_{min,0}, N_{max,0}] = [1, 10N_{TOT}]$. Spread the assigned numbers ($N_{min,0}, N_{max,0}$) of objects over the circular domain, as shown in Fig. 2a and obtain the original densities p_{min} and p_{max} (colored+gray). Initially, the range $[p_{min}, p_{max}]$ is assigned to be very wide ($\approx [0, 1]$) which ensures that it contains the percolation threshold p_c . Meanwhile, the percolation threshold p_c corresponds to the appropriate original number of ellipses N in the range of $[N_{min,0}, N_{max,0}]$, hence:

$$N \in [N_{min,0}, N_{max,0}]$$

In the next steps, we will narrow-down the percolation threshold p_c with the desired precision.

1. Having the original ellipses range of $[N_{min,k}, N_{max,k}]$ in the step k , calculate the percolation possibility for the middle of the range \bar{N}_k :

$$\bar{N}_k \approx \frac{N_{min,k} + N_{max,k}}{2} \tag{22}$$

where in the initial step $\bar{N}_0 \approx 5N_{TOT}$, and the approximation sign is used to round into the nearest integer. Similarly spread the assigned average original number of ellipses \bar{N}_k into the medium and compute the obtained average original density \bar{p}_k . Subsequently check percolation to the boundaries.

2. If there is a connection to the boundary the average original ellipse number \bar{N}_k , is larger than the needed numbers for percolation. In that case, it is chosen to be the new upper bound for the next iteration (i.e. $N_{max,k+1} := \bar{N}_k$), otherwise it is not enough to achieve percolation, in which case it is chosen as the new lower bound in the next iteration (i.e. $N_{min,k+1} := \bar{N}_k$), as below:

$$\text{Check } \bar{N}_k \text{ for percolation : } \begin{cases} \text{Success (i.e. 1)} & N \in [N_{min,k}, \bar{N}_k] \\ \text{Failure (i.e. 0)} & N \in [\bar{N}_k, N_{max,k}] \end{cases} \tag{23}$$

where 1 means touching the boundary and 0 means otherwise. Hence the range of the number of ellipses N for the existence of the percolation threshold is halved in every consecutive iteration step k . Due to stochasticity, the confidence for locating the upper/lower boundary needs to be increased, so the critical density would not get accidentally missed out when iterating for a special arrangement of the particulates. In order to avoid such cases, the connection check for the middle value \bar{N} has been performed 11 times and the

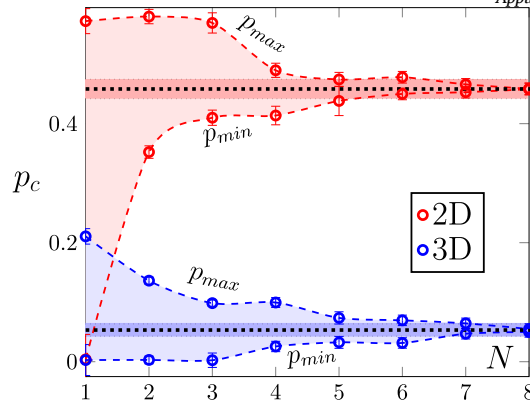


Fig. 4. Illustration of the gradual convergence of the maximum p_{max} and minimum p_{min} versus the consecutive iterations N , to the percolation threshold p_c , where finally $\bar{p} \approx p_{max} \approx p_{min}$ and leads to $p_{c,3} \approx 0.295 \pm 0.046$, $p_{c,2} \approx 0.505 \pm 0.030$ using half-interval search in the original number of ellipses N for 2 and 3 dimensions. ($\rho_0 = 0.004$, $r = 0.5$) The convergence maximum error threshold has been assigned as 0.0005.

resulting event (i.e. 0 or 1) with higher multiplicity is selected as the new upper/lower boundary. This will locally increase the confidence in choosing the appropriate half to continue with. As an example, the case of $[11010111011]$ is considered to be a percolation event ($\rightarrow 1$) and the case of $[01010101010]$ is interpreted as no percolation ($\rightarrow 0$), the latter being very close to final percolation threshold since the number of 0s and 1s are comparable. In fact, in the event of getting the mixed outcome of similar repetitions for 0 and 1, the explored boundary value should be near the percolation threshold p_c already and choosing any half should lead to similar outcome.

3. Repeat the steps 1 and 2 for halving the range of original number of ellipses $[N_{min,k}, N_{max,k}]$. Hence for every iteration k , spreading the minimum and maximum number of particles in this range over the medium, in average will generate the original density range $[p_{min,k}, p_{max,k}]$, as below:

$$N_{min,k} \leq N \leq N_{max,k} \Rightarrow p_{min,k} \leq p_c \leq p_{max,k} \tag{24}$$

4. Stop the iteration when the bounds of the obtained interval for the original density become close enough, with the assigned precision Err , such that $|p_{max,k} - p_{min,k}| \leq Err$. The error value Err could be small enough based on the required number of digits. As an example $Err = 0.0005$ could satisfy the precision up to 3 digits. Hence, the original density values in the boundaries approach enough together and the percolation value can be determined as:

$$p_{min,k} \approx p_{max,k} \rightarrow p_c \tag{25}$$

Due to stochasticity, each run for percolation threshold p_c was repeated 10 times to improve the confidence interval and bypass the exceptional case scenarios. Fig. 4 illustrates a convergence process for the elemental density $\rho_0 = 0.004$ and the aspect ratio $r = 0.5$, where average and standard deviations of the local (each point from 5 runs) and global (from 10 runs) are visualized.

As observed, the error bars for this specific range of parameters are quite small (i.e. in 2D the first iteration for p_{max} gets 0.639 ± 0.021 which shows the variation of 3.3%). Hence, increasing the number of repetitions in this case with additional computational cost might not add more information, while a larger error bar values would have required higher number of repetitions. Thus, the percolation threshold p_c is obtained with the required precision.

As well, one should note that the obtained p_c here is specific to the rigid boundary condition. However, if the periodic boundary condition (PBC) was assumed (either spanning or wrapping boundary condition), the possibility of a connection would increase and the obtained percolation threshold value p_c would become smaller [46,58].

Note that, in the case that $N_{min,k}$ and $N_{max,k}$ are not updated, a new random placement of ellipses is performed and the obtained original density $p_{min,k}$ or $p_{max,k}$, might be slightly different (higher or lower) from the previous step with the same number of ellipses.

Steps 1 to 3 could get performed via assigning the original density values p_{min} and p_{max} instead of the original number of ellipses N_{min} and N_{max} . In such a case, the procedure for targeting the desired original density p based on search for the appropriate number of ellipses N is explained in the next section.

Table 2 compares the obtained values through the developed model, with the popular FSS method. Note that while FSS method is based on the end-to-end percolation possibility in a planar medium, the current study explores the center-to-end percolation in a circular medium, where the central particle is already prescribed. Hence, one should expect some degree of difference in the percolation thresholds predicted by this study and the existing literature.

2.5. Connection density ρ

Given a dispersed medium of the elliptic particulates with the original areal/volumetric density p , the propagating cluster starts from the prescribed central element as the seed and grows through overlaps toward the border of the rounded domain. Such cluster

Table 2
Comparison of the current model with the previous studies using finite size scaling method.

Geometry	r	This Study		Literature	\bar{Err}
		ρ_0	p_c	p_c	
Sphere	1	0.004	0.283 ± 0.013	0.289 [59], 0.2896 [56], 0.2895 [46]	$\approx 2\%$
Prolate	0.5	0.002	0.265 ± 0.015	0.262 [60]	$\approx 1\%$
	0.25	0.016	0.167 ± 0.026	0.16 [61]	$\approx 4\%$
Oblate	0.5	0.002	0.271 ± 0.015	0.263 [60]	$\approx 3\%$
	0.25	0.002	0.194 ± 0.018	0.200 [60]	$\approx 3\%$

has a certain connected density ρ (i.e. $0 \leq \rho \leq 1$) and a reach, which is maximum possible distance from the center to the boundary of the propagating connected cluster (i.e. $0 \leq reach \leq R$) and R is the radius of the domain).

In order to characterize the correlation of the maximum density difference $\Delta\rho_{max}$ versus the difference in the percolation threshold Δp_c , for every simulation one would need to vary the original density p in the range of the corresponding percolation thresholds, where:

$$p_{c,3} \leq p \leq p_{c,2} \tag{26}$$

For this range, one could generate the percolation case scenario with the desired original density p . The minimum number of required original particles N occurs in ideal case of no overlaps (i.e. pN_{TOT}). Hence, one can start from this number, randomly disperse the particles, and compute the obtained density p_k . In the presence of the overlaps, one has $p_k < p$. In such case, we repetitively increase the original number of ellipses (i.e. $N_{k+1} := N_k + 1$), until approaching the original density p with the desired precision and anticipated error threshold Err , as follows:

$$|p - p_k| < Err \tag{27}$$

where the threshold value in this case was taken to be $Err = 0.0005$. There could be exceptional circumstances for which the projected values of p_k and p_{k+1} in two consecutive runs are too different and neither of them satisfy Equation (27). In such cases, the program (i.e. while loop) was repeatedly re-run from the beginning, until Equation (27) became satisfied. Algorithm 1 summarizes the mentioned steps as pseudo-code, where the upper limit of the number of ellipses N_{max} for stopping and re-running the program has been taken as 10 times the total number of domain-covering ellipses, with no-overlaps ($N_{max} := 10N_{TOT}$).

Algorithm 1 Targeting the desired original density p via the handle of number of ellipses N_k .

Pseudocode	Explanation
$k := 1$ $N_k := pN_{TOT}$ \rightarrow Compute p_1	Try initially to get p from the case of no overlaps.
While $ p - p_k > Err$ $\rightarrow N_{k+1} := N_k + 1$	Increase the number of ellipses N_k by 1.
$k = k + 1$ \rightarrow Compute p_k	Find the new original density p_k .
if $N_k = 10N_{TOT}$ $\rightarrow N_k := pN_{TOT}$	If the density is missed-out, try from beginning.
End	

The continuum percolation algorithm ($N \rightarrow p \rightarrow \rho$) is described as follows:

1. The N_k number of ellipsoids are generated with the variation in the prescribed elemental density values $\rho_0 \in \{2^1, 2^2, 2^3, 2^4, 2^5, 2^6\} \times 10^{-3}$ and that of the aspect ratio values $r \in \{0.125, 0.25, 0.5, 0.75, 0.875, 1$ (sphere)} as listed in the Table 3. The axial dimensions of a_1, a_2 (and a_3) are calculated from the equations in Table 1, which form prolate (i.e. $(1, r, r)$) and oblate (i.e. $(1, 1, r)$) ellipsoids. For each ellipsoid, two of the three rotation angles are given random values (i.e. $\alpha_i \in [0, 2\pi]$) and its coordinates are rotated using the rotation matrix in Equation (6).

2. The ellipsoids are randomly dispersed into central locations $x_{0,i} \in \left[-\frac{l}{2}, \frac{l}{2}\right]$, such that they remain inside the circle centered at the origin with a radius of $\frac{l}{2}$. Hence:

$$\sqrt{x_{0,1}^2 + x_{0,2}^2 + x_{0,3}^2} \leq \frac{l}{2} \tag{28}$$

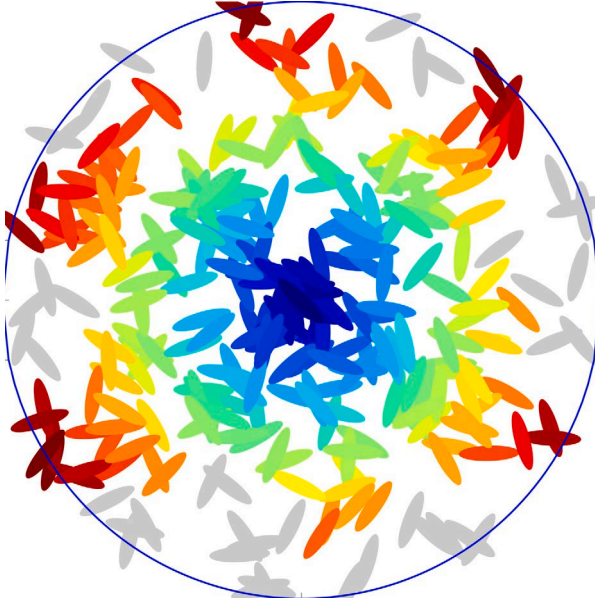
3. The adjacency matrix $\Gamma_{N_k \times N_k}$ is created based on the algorithm presented in the subsection 2.3.

4. In order to ensure the instigation of percolation, the first elliptic particulate is placed in the center (i.e. $\mathbf{X}_1 = 0$) as the seed element, with a random orientation. Subsequently, continuum percolation is performed through the connected pathways (i.e. overlaps), until no further progress can be made. The obtained cluster at each iteration becomes a subset of the original dispersed ellipses. Figs. 5a and 5b illustrate samples of center-initiated percolation clusters in 2 and 3 dimensions respectively.

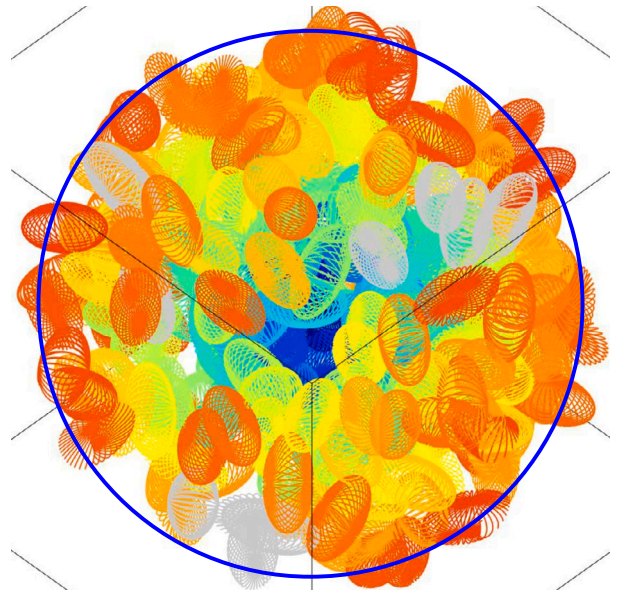
5. The original density p , as well as the density of each connected cluster ρ can be obtained via gridding the medium into multitudes of points (i.e. $N_{dots} = 100^n$ where n is the dimension of the domain) with finite spacing, and counting the portion of the enclosed

Table 3
Simulation parameters.

r	$\rho_0 (\times 10^{-3})$	l	N	Repetitions	N_{dots}
{0.125, 0.25, 0.5, 0.75, 0.875, 1}	{ $2^1, 2^2, 2^3, 2^4, 2^5, 2^6$ }	1	$\left[1, \frac{10}{\rho_0}\right]$	$\times 11$ (point), $\times 10$ (run)	100^n



(a) 2D Clustering for the elemental density $\rho_0 = 0.002$, aspect ratio $r = 0.25$, and given number of ellipses $N = 375$.



(b) 3D Clustering for the elemental density $\rho_0 = 0.004$, aspect ratios $r = 0.5$, and the given number of ellipses ($N = 88$).

Fig. 5. The center-initiated percolation samples, reaching the boundary of the 2 and 3 dimensional domains. The color range, from blue to red, commensurates with the distance (i.e. number of iterations steps) from the center and the gray color shows the disconnected ellipses.

points falling within either entire ellipses (V) or the connected cluster (V_{Clus}). Hence, similar to step 3, for the point to fall inside the connected cluster, it should satisfy Equation (16). Fig. 6 visualizes such points, inside either the connected cluster (color) or separated ellipsoids (gray). Hence all the inner points are counted (for overlaps, only once).

6. The density of the connection cluster ρ is obtained via dividing its obtained volume (V_{Clus}) by the total volume (V_{TOT}) coverage of the domain, as shown in Equation (9).

The prescribed variation in the element geometry r , as well as the elemental density ρ_0 determines the density of the connected cluster ρ (steps 1 to 6). This causes disparity in the 2D-3D difference of the percolation threshold Δp_c and consequently in the difference of the maximum 2D-3D difference in cluster densities $\Delta \rho_{max}$, as schematically illustrated earlier in the Fig. 3. Fig. 7 illustrates such correlation, where for each original density value, 10 runs were performed, and their average and standard deviations were determined.

3. Results & discussions

The pattern of convergence to the percolation threshold p_c for connecting the center to the border which is shown in the Fig. 4 necessitates the involvement of (at least) one overlapping chain of elements, with a specific individual scale (i.e. ρ_0) and the number involved in the cluster chain N_{Clus} which is a subset of original number of elements N (i.e. $N_{Clus} \leq N$). Typically, the larger the particle size ($\rho_0 \uparrow$), the fewer number of ellipses are needed for the connection ($N_{Clus} \downarrow$), and in order to maintain the percolation threshold one has:

$$\rho_0 \sim \frac{1}{N_{Clus}} \tag{29}$$

In particular, if the elemental density ρ_0 becomes very large, only a small number of ellipses are needed for percolation. In such a case, the effect of individual particles (i.e. orientation α_i , axis size a_i), becomes more pronounced for determining the extent of the connected cluster ρ and the possibility of full percolation (i.e. touching the boundaries). Since such orientations in-particular are randomly assigned, the percolation in such finite systems will become more stochastic and the error range will grow. Conversely if the elemental density is relatively small, the required number of ellipses for percolation becomes large, and cluster-level behavior (i.e. placements of particle) becomes more important in determining the extent of percolation.

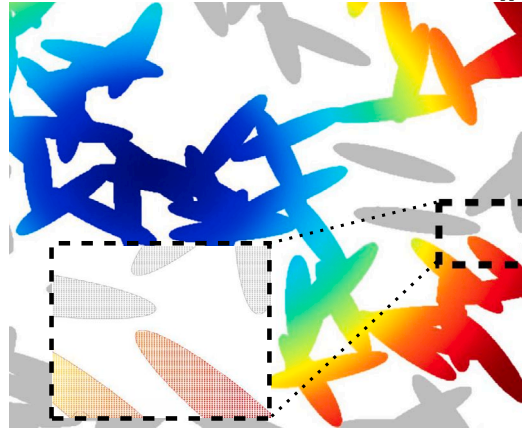


Fig. 6. Illustration of counting the enclosed grid points for computing the cluster connection density ρ , where it could get computed from the fractions of enclosed dots in the connected chains (in color). The zoomed area facilitates noting the enclosed grid points.

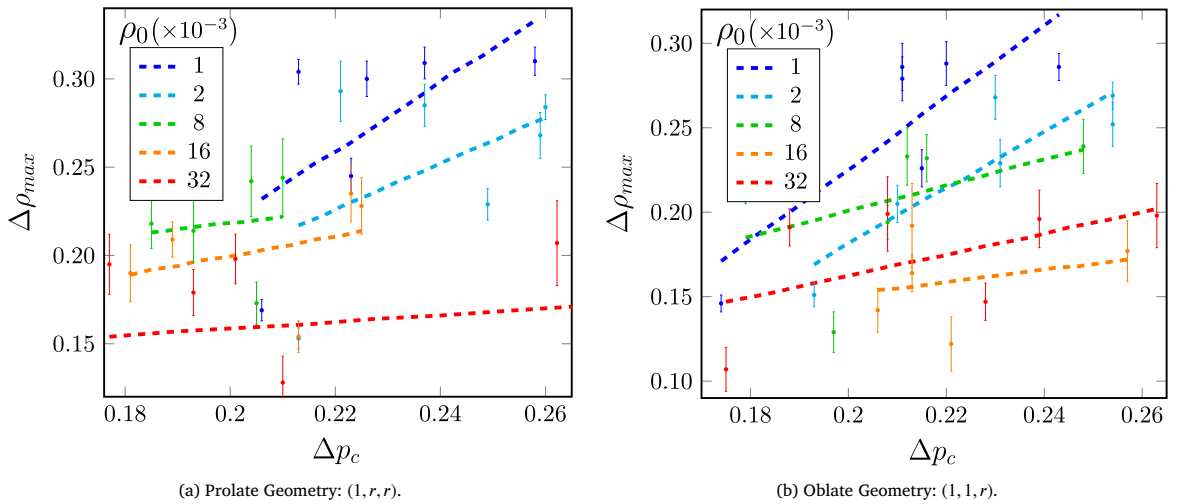


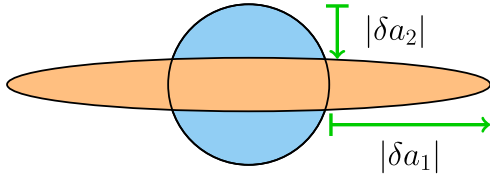
Fig. 7. The correlation of the maximum 2D-3D difference in the connection density $\Delta\rho_{max}$ versus the 2D-3D difference in the percolation thresholds Δp_c for (a) Prolate (i.e. $(1, r, r)$) and (b) Oblate (i.e. $(1, 1, r)$) geometries, which is obtained through varying the aspect ratio r , for multitudes of original elemental density values $\rho_0 \in \{1, 2, 8, 16, 32\} \times 10^{-3}$. The dashed lines represent the linear regression fitting where the positive slope, illustrates the direct correlation between the axis.

Following on from the divergence and convergence trends, explained earlier in the Fig. 3, the correlation between the 2D-3D difference in the percolation thresholds Δp_c versus the maximum 2D-3D difference in the connection densities $\Delta\rho_{max}$ is explored numerically. In this regard, sweeping the original density p in the range of the percolation thresholds $p_{c,3} < p < p_{c,2}$, the individual connection densities ρ and their overall maximum difference across the range $\Delta\rho_{max} = \rho_3 - \rho_2$ is computed. Such correlation, which is specific to the aspect ratio r and the elemental density ρ_0 , was run 10 times and the average and standard deviations are presented in the Figs. 7a and 7b for both prolate $(1, r, r)$ and oblate $(1, 1, r)$ geometries respectively. Subsequently, linear interpolation (i.e. dashed lines) was performed, where the positive slopes make such correlation evident. Hence:

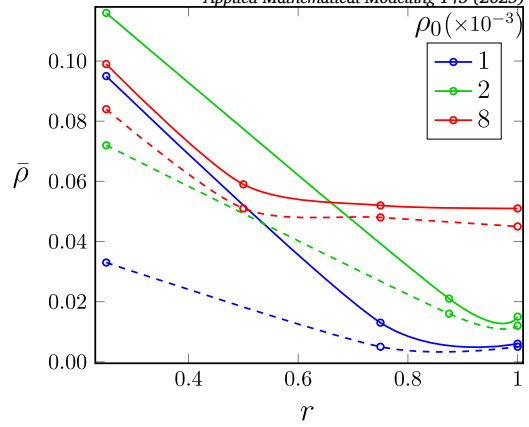
$$\Delta\rho_{max} \sim \Delta p_c \tag{30}$$

This correlation could be qualitatively explained visually from the schematic of estimated 2D and 3D density trends, illustrated earlier in Fig. 3. Comparing the corresponding differences in 2D and 3D density when moving along the actual calculated trend curves from $(0, 0)$ to $(1, 1)$, one can focus on the highlighted zone of difference which starts from a divergence stage, and ends at a convergence stage. This zone roughly resembles a diamond, where any horizontal enlargement in the width (i.e. $\Delta p_c \uparrow$) should lead to growth in the height (i.e. $\Delta\rho_{max} \uparrow$) as well. Conversely, when the 2D and 3D trends almost lie on each other $\Delta p_c \rightarrow 0$ and therefore $\Delta\rho_{max} \rightarrow 0$.

Additionally, one could compare the rate of the growth in connection density ρ versus the change in the original density p , between the 2D and 3D percolation systems. Defining such rate as $m := \frac{\partial\rho}{\partial p}$, one could discern that in the earlier divergence zone the 3D percolation system picks up with faster rate. Conversely, in the later convergence zone, the 2D percolation system grows with a faster rate, and catches up. This can be summarized as follows:



(a) The effect of particle geometry on the reach: When particle volume (elemental density ρ_0) is conserved, a larger elongation in the major axis ($|\delta a_1|$) occurs in the expense of a lower shrinkage in the minor axis ($|\delta a_2|$).



(b) The average connection density $\bar{\rho}$ for the prolate (solid), versus the oblate (dashed) ellipsoid geometries. The original number of particles is chosen as half of the saturating non-overlapping case: $N := 0.5N_{TOT}$ (rounded).

Fig. 8. The role of the element shape (controlled by aspect ratio r) on the obtained average connected density $\bar{\rho}$ which commensurates with the reach of the individual objects (i.e. local) and the connected cluster (i.e. global). In the largest limit as the aspect ratio tends to 1 ($r \rightarrow 1$), both prolate ($1, r, r$) and oblate ($1, 1, r$) geometries become a sphere, and the obtained average connection densities $\bar{\rho}$ converge to each other.

$$\begin{cases} \bar{m}_{3D} > \bar{m}_{2D} & \text{Divergence Zone} \\ \bar{m}_{3D} < \bar{m}_{2D} & \text{Convergence Zone} \end{cases} \quad (31)$$

where the overbar on a symbol stands for the average value, to avoid exceptional cases due to stochasticity.

An effective factor for the connectedness of the ellipsoid particulates is their shape while conserving the volume, which is defined for an ellipsoid of axes a_1, a_2 and a_3 as:

$$V = \frac{4}{3}\pi a_1 a_2 a_3 \quad (32)$$

Since $\delta V = 0$, one could investigate the reach the particle, using the relative variations in the axis a_i . Hence, the differential form yields:

$$\frac{\delta a_1}{a_1} + \frac{\delta a_2}{a_2} + \frac{\delta a_3}{a_3} = 0 \quad (33)$$

which means that a relative increase in each axis should be compensated by a relative decrease in the other directions. Such relative correlation means a higher change for the larger axis ($|\delta a_i| \propto a_i$) which increases the reach of the connected cluster to a greater extent, than decreasing it in the other directions, as shown in the Fig. 8a. Hence overall, the extent of the connection increases. This is the underlying reason for higher connection propensity in the prolate shapes ($1, r, r$) than in their oblate counterparts ($1, 1, r$). The simulation results in the Fig. 8b show the analogous trend where in the limit of $r \rightarrow 1$ the average connection density values $\bar{\rho}$ converge since both shapes merge to a sphere. Such invariance to the shape (i.e. r), particularly has recently been investigated in 2D for the ratio of normalized density of particles in the connected cluster to the percolation threshold (i.e. $\hat{\rho} := \frac{\rho}{\rho_c}$) to the relative strain in the number of particles from the percolation state (i.e. $\epsilon := \frac{N - N_c}{N_c}$) [62], illustrating the independence from the eccentricity (i.e. shape factor). The correlation is obtained to be nearly parabolic in $\log \epsilon$ (Figure 5a in the aforementioned paper), and can be represented by the following form:

$$\hat{\rho} = C_1 + C_2 \log \epsilon + C_3 (\log \epsilon)^2$$

Using our procedure, we have investigated such a correlation by computing the defined variables $\hat{\rho}$ versus ϵ (10 times for a point) using the entire span of the aspect ratios $r \in \{0.125, 0.25, 0.5, 0.75, 0.875, 1\}$, to ensure a wide range of eccentricity. The interpolating coefficients for the selected values of the original densities ρ_0 are obtained as:

		$C_1(r)$	$C_2(r)$	$C_3(r)$
ρ_0	0.002	0.640 ± 0.058	0.264 ± 0.014	0.039 ± 0.003
	0.004	0.622 ± 0.069	0.264 ± 0.018	0.039 ± 0.003

Since the standard deviations are significantly smaller than the average values of the corresponding coefficients (particularly for the linear and parabolic terms), one can conclude that the correlations are nearly independent of the particle shape ($C_i(r) \approx C_i$) for the selected original densities.

Note that, while the simulations in this paper were carried out using the rigid boundary condition, adopting the periodic boundary condition is expected to lead to qualitatively similar trends, albeit quantitatively different. As well, utilizing normalized parameters,

such as elemental density (i.e. $\rho_0 = \frac{V_0}{V_{TOT}}$), original density (i.e. $p = \frac{V}{V_{TOT}}$) and the connected density (i.e. $\rho = \frac{V_{Clus}}{V_{TOT}}$), makes the characterizations applicable to any domain size.

4. Conclusions

In this work, we have developed center-initiated continuum percolation procedures via the elliptic fillers in 2 and 3 dimensions. After defining a 2D-3D equivalence for original density p , we initially developed a new iterative method to compute the percolation threshold p_c in finite systems versus the elemental density ρ_0 and the aspect ratio r . Subsequently, we established an efficient computational methodology to discern the connected cluster and compute its density ρ . Finally, we characterized the maximum 2D-3D difference in density of the connection cluster $\Delta\rho_{max}$, and successfully correlated that to the 2D-3D difference in the percolation thresholds Δp_c . Furthermore, we have compared 2D and 3D percolation models, in terms of the rate of variation in the connection density ρ versus the original density p . Finally, we addressed the role of the shape parameters on the reach for prolate and oblate geometries, which was verified through computing the connected density ρ for a series of aspect ratios r and elemental density ρ_0 . The results could be useful for efficient percolation design based on thick (3D) versus thin (2D) composite layers in terms of the geometrical parameters as well as the elemental density.

CRedit authorship contribution statement

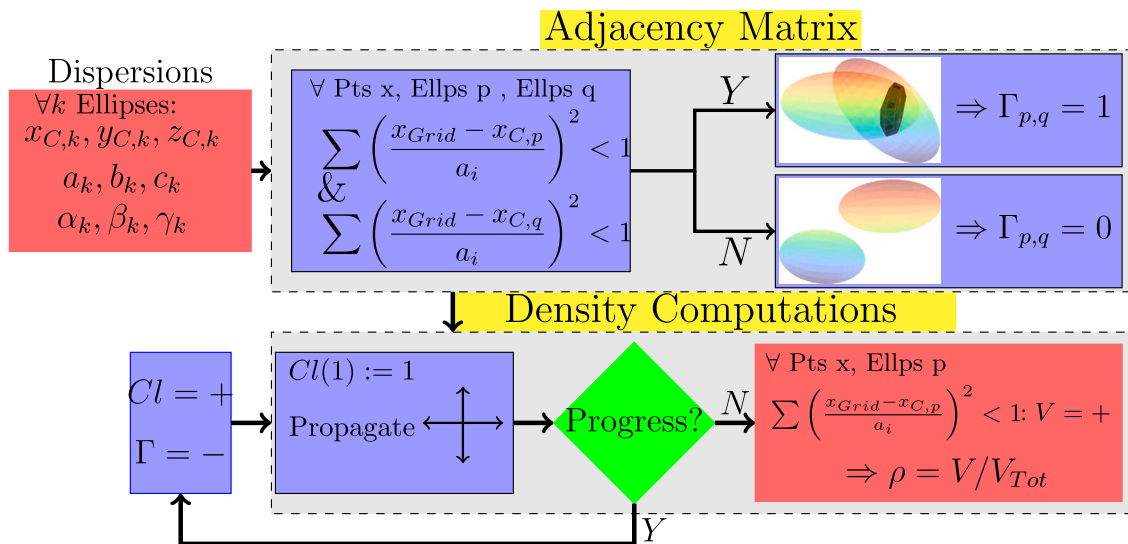
Asghar Aryanfar: Writing – review & editing, Writing – original draft, Visualization, Validation, Software, Methodology, Investigation, Formal analysis, Data curation, Conceptualization. **Mahmoud Yamani:** Writing – original draft, Validation, Software, Formal analysis, Data curation. **William A. Goddard:** Supervision, Project administration.

Declaration of competing interest

The authors declare that they have no known competing financial interests or personal relationships that could have appeared to influence the work reported in this paper.

Appendix A

The pseudo-chart for computing the densities via the overlaps have been visualized in the Figure below:



Pseudo-chart for calculating the percolation thresholds p_c and connected densities ρ , Ellipses: number of ellipses; $x_{C,k}, y_{C,k}, z_{C,k}$: the central coordinates for the ellipse k ; a_k, b_k, c_k and $\alpha_k, \beta_k, \gamma_k$: scales and rotations of the axis in the respective directions; $\Gamma_{p,q}$: adjacency matrix value for the ellipses p, q ; Cl : the connected cluster of ellipses, V : the number of the grid points falling inside the cluster of ellipses, V_{TOT} : the total number of grid points; ρ : the density of the propagating connected cluster.

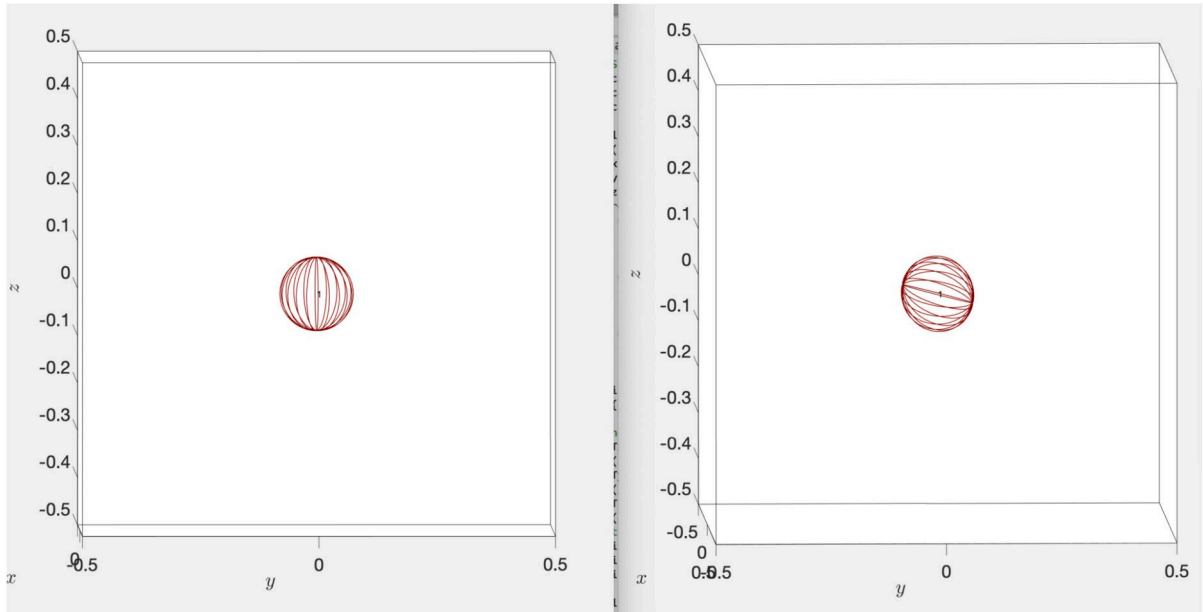
Appendix B

The rotation matrix has been expressed in terms of 3 distinct rotations α_1, α_2 and α_3 around the axis x, y, z . We verify their individual positive (right-handed) rotations visually as below.

1. Rotation around axis x :

$$R_x = \begin{bmatrix} 1 & 0 & 0 \\ 0 & \cos \alpha_1 & -\sin \alpha_1 \\ 0 & \sin \alpha_1 & \cos \alpha_1 \end{bmatrix}$$

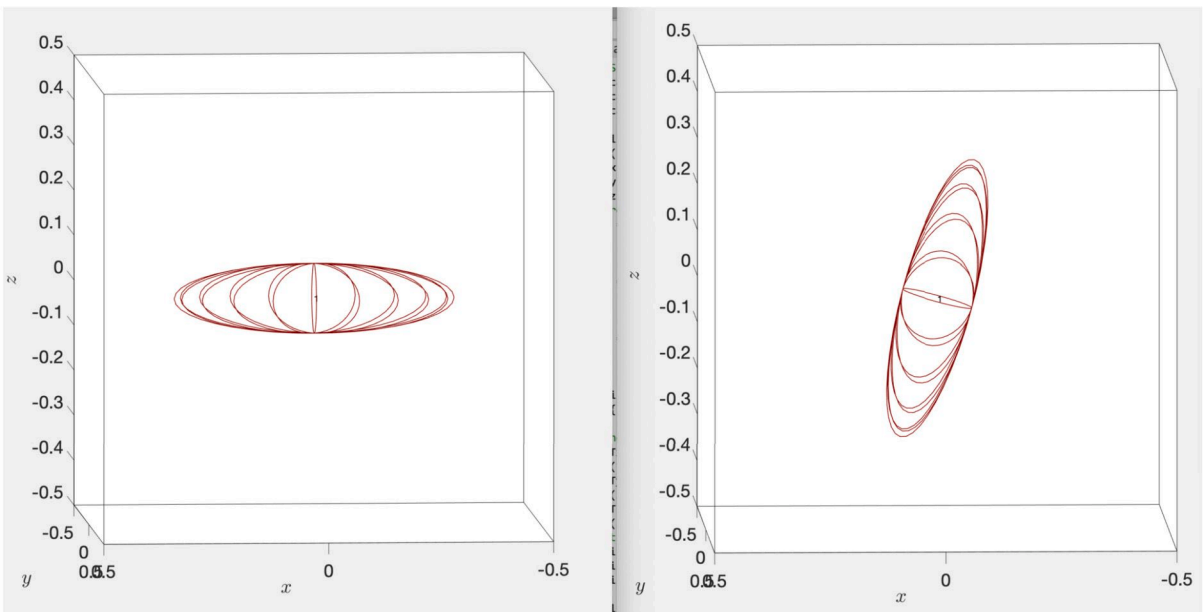
which yields:



Left: Original, Right: $\alpha_1 = 80^\circ$ ✓

2. Rotation around axis y :

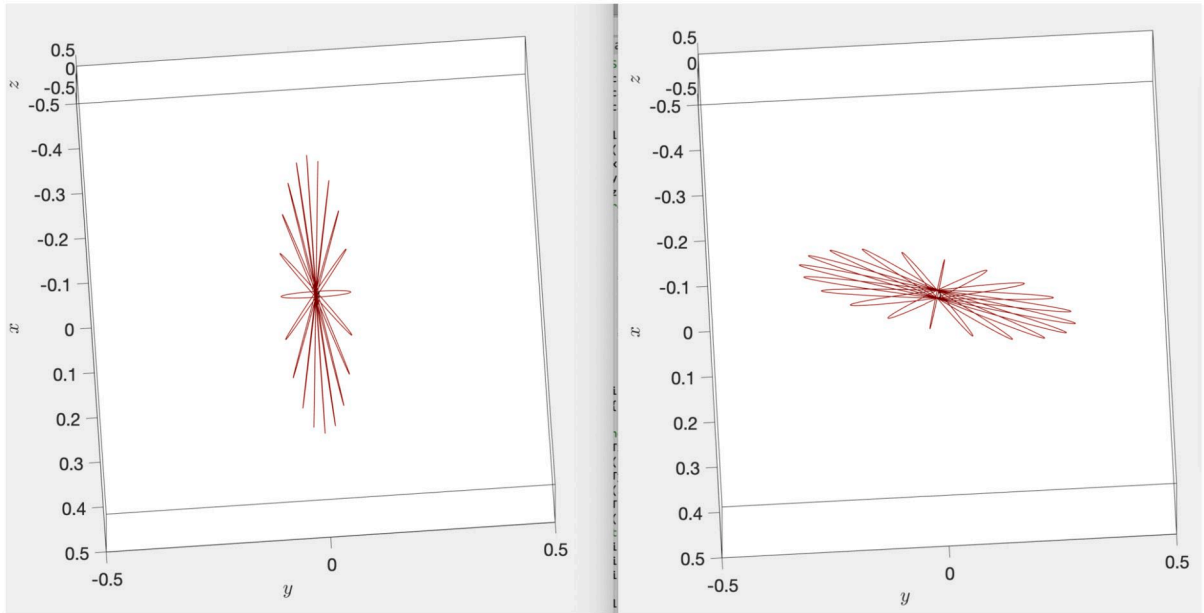
$$R_y = \begin{bmatrix} \cos \alpha_2 & 0 & \sin \alpha_2 \\ 0 & 1 & 0 \\ -\sin \alpha_2 & 0 & \cos \alpha_2 \end{bmatrix}$$



Left: Original, Right: $\alpha_2 = 80^\circ$ ✓

2. Rotation around axis z:

$$R_z = \begin{bmatrix} \cos \alpha_3 & -\sin \alpha_3 & 0 \\ \sin \alpha_3 & \cos \alpha_3 & 0 \\ 0 & 0 & 1 \end{bmatrix}$$



Left: Original, Right: $\alpha_3 = 80^\circ$ ✓

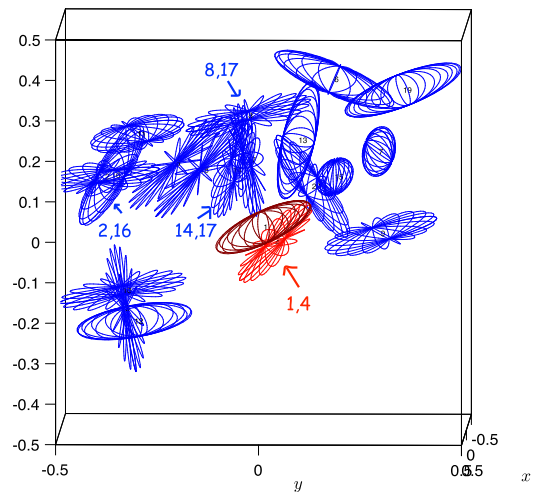
Appendix C

Below, we provide two examples for visualization of ellipsoids intersections and checking the accuracy of the adjacency matrix:

- $N_{EI} = 20$ (crowded example)

Variables - Adj																				
Adj																				
20x20 logical																				
	1	2	3	4	5	6	7	8	9	10	11	12	13	14	15	16	17	18	19	20
1	0	0	0	1	0	0	0	0	0	0	0	0	0	0	0	0	0	0	0	0
2	0	0	0	0	0	0	0	0	0	0	0	0	0	0	0	0	0	0	0	0
3	0	0	0	0	0	0	0	0	0	0	0	0	0	0	0	0	0	0	0	0
4	1	0	0	0	0	0	0	0	0	0	0	0	0	0	0	0	0	0	0	0
5	0	0	0	0	0	0	0	0	0	0	0	0	0	0	0	0	0	0	0	0
6	0	0	0	0	0	0	0	0	0	0	0	0	0	0	0	0	0	0	0	0
7	0	0	0	0	0	0	0	0	0	0	0	0	0	0	0	0	0	0	0	0
8	0	0	0	0	0	0	0	0	0	0	0	0	0	0	0	0	0	0	0	0
9	0	0	0	0	0	0	0	0	0	0	0	0	0	0	0	0	0	0	0	0
10	0	0	0	0	0	0	0	0	0	0	0	0	0	0	0	0	0	0	0	0
11	0	0	0	0	0	0	0	0	0	0	0	0	0	0	0	0	0	0	0	0
12	0	0	0	0	0	0	0	0	0	0	0	0	0	0	0	0	0	0	0	0
13	0	0	0	0	0	0	0	0	0	0	0	0	0	0	0	0	0	0	0	0
14	0	0	0	0	0	0	0	0	0	0	0	0	0	0	0	0	0	0	0	0
15	0	0	0	0	0	0	0	0	0	0	0	0	0	0	0	0	0	0	0	0
16	1	0	0	0	0	0	0	0	0	0	0	0	0	0	0	0	0	0	0	0
17	0	0	0	0	0	0	0	1	0	0	0	0	0	0	0	0	0	0	0	0
18	0	0	0	0	0	0	0	0	0	0	0	0	0	0	0	0	0	0	0	0
19	0	0	0	0	0	0	0	0	0	0	0	0	0	0	0	0	0	0	0	0
20	0	0	0	0	0	0	0	0	0	0	0	0	0	0	0	0	0	0	0	0

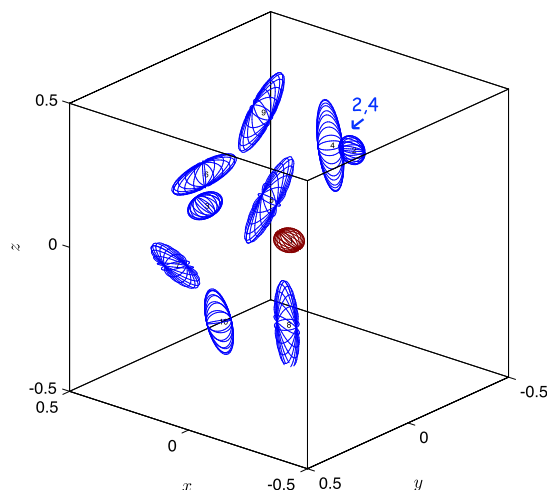
The obtained Adjacency Matrix $\Gamma_{i,j}$



Visualization of Ellipsoids

- $N_{EI} = 10$ (clear example)

Adj		1	2	3	4	5	6	7	8	9	10
1	0	0	0	0	0	0	0	0	0	0	0
2	0	0	0	1	0	0	0	0	0	0	0
3	0	0	0	0	0	0	0	0	0	0	0
4	0	1	0	0	0	0	0	0	0	0	0
5	0	0	0	0	0	0	0	0	0	0	0
6	0	0	0	0	0	0	0	0	0	0	0
7	0	0	0	0	0	0	0	0	0	0	0
8	0	0	0	0	0	0	0	0	0	0	0
9	0	0	0	0	0	0	0	0	0	0	0
10	0	0	0	0	0	0	0	0	0	0	0

The obtained Adjacency Matrix $\Gamma_{i,j}$ 

Visualization of Ellipsoids

Appendix D. Supplementary material

Supplementary material related to this article can be found online at <https://doi.org/10.1016/j.apm.2025.116007>.

Data availability

The raw data for producing the results in this manuscript are freely available upon request from the corresponding author at aryanfar@caltech.edu.

References

- [1] M. Sahini, Muhammadpr Sahimi, Applications of Percolation Theory, CRC Press, 1994.
- [2] Omar Malik, Xiangyi Meng, Shlomo Havlin, Gyorgy Korniss, Boleslaw Karol Szymanski, Jianxi Gao, Concurrence percolation threshold of large-scale quantum networks, Commun. Phys. 5 (1) (2022) 1–11.
- [3] Vinod K.S. Shante, Scott Kirkpatrick, An introduction to percolation theory, Adv. Phys. 20 (85) (1971) 325–357.
- [4] Russell Lyons, Random walks, capacity and percolation on trees, Ann. Probab. (1992) 2043–2088.
- [5] József Balogh, Yuval Peres, Gábor Pete, Bootstrap percolation on infinite trees and non-amenable groups, Comb. Probab. Comput. 15 (5) (2006) 715–730.
- [6] Paul N. Suding, Robert M. Ziff, Site percolation thresholds for Archimedean lattices, Phys. Rev. E 60 (1) (1999) 275.
- [7] Fumiko Yonezawa, Shoichi Sakamoto, Motoo Hori, Percolation in two-dimensional lattices. I. A technique for the estimation of thresholds, Phys. Rev. B 40 (1) (1989) 636.
- [8] Jianjun Lin, Huisu Chen, Wenxiang Xu, Geometrical percolation threshold of congruent cuboidlike particles in overlapping particle systems, Phys. Rev. E 98 (1) (2018) 012134.
- [9] H-P. Hsu, M-C. Huang, Percolation thresholds, critical exponents, and scaling functions on planar random lattices and their duals, Phys. Rev. E 60 (6) (1999) 6361.
- [10] John W. Essam, Percolation theory, Rep. Prog. Phys. 43 (7) (1980) 833.
- [11] Allen Hunt, Robert Ewing, Behzad Ghanbarian, Percolation Theory for Flow in Porous Media, vol. 880, Springer, 2014.
- [12] M. Sahimi, Hydrodynamic dispersion near the percolation threshold: scaling and probability densities, J. Phys. A, Math. Gen. 20 (18) (1987) L1293.
- [13] Roey Nativ, Michael Shtein, Gal Shachar, Maxim Varenik, Oren Regev, Optimal nanomaterial concentration: harnessing percolation theory to enhance polymer nanocomposite performance, Nanotechnology 28 (30) (2017) 305701.
- [14] Chandong Sheng, J.L.T. Azevedo, Modeling biomass devolatilization using the chemical percolation devolatilization model for the main components, Proc. Combust. Inst. 29 (1) (2002) 407–414.
- [15] Miguel A. Aon, Sonia Cortassa, Brian O'Rourke, Percolation and criticality in a mitochondrial network, Proc. Natl. Acad. Sci. 101 (13) (2004) 4447–4452.
- [16] Asghar Aryanfar, Sajed Medlej, Ali Tarhini, et al., Elliptic percolation model for predicting the electrical conductivity of graphene-polymer composites, Soft Matter 17 (8) (2021) 2081–2089.
- [17] Wenxiang Xu, Mingkun Jia, Zheng Gong, Thermal conductivity and tortuosity of porous composites considering percolation of porous network: from spherical to polyhedral pores, Compos. Sci. Technol. 167 (2018) 134–140.
- [18] Wenxiang Xu, Yufeng Zhang, Jinyang Jiang, Zhiyong Liu, Yang Jiao, Thermal conductivity and elastic modulus of 3d porous/fractured media considering percolation, Int. J. Eng. Sci. 161 (2021) 103456.
- [19] Wenxiang Xu, Yang Jiao, Theoretical framework for percolation threshold, tortuosity and transport properties of porous materials containing 3d non-spherical pores, Int. J. Eng. Sci. 134 (2019) 31–46.
- [20] Wenxiang Xu, Peng Lan, Yaqing Jiang, Dong Lei, Haixia Yang, Insights into excluded volume and percolation of soft interphase and conductivity of carbon fibrous composites with core-shell networks, Carbon 161 (2020) 392–402.
- [21] Abbas Ali Saberi, Recent advances in percolation theory and its applications, Phys. Rep. 578 (2015) 1–32.
- [22] Łukasz Kurzwaski, Krzysztof Malarz, Simple cubic random-site percolation thresholds for complex neighbourhoods, Rep. Math. Phys. 70 (2) (2012) 163–169.

- [23] Kathleen E. Hamilton, Leonid P. Pryadko, Tight lower bound for percolation threshold on an infinite graph, *Phys. Rev. Lett.* 113 (20) (2014) 208701.
- [24] Yasser Zare, An approach to study the roles of percolation threshold and interphase in tensile modulus of polymer/clay nanocomposites, *J. Colloid Interface Sci.* 486 (2017) 249–254.
- [25] Ali Al-Dahawi, Mohammad Haroon Sarwary, Oğuzhan Öztürk, Gürkan Yıldırım, Arife Akın, Mustafa Şahmaran, Mohamed Lachemi, Electrical percolation threshold of cementitious composites possessing self-sensing functionality incorporating different carbon-based materials, *Smart Mater. Struct.* 25 (10) (2016) 105005.
- [26] Hyun-Jung Choi, Moo Sung Kim, Damiro Ahn, Sang Young Yeo, Sohee Lee, Electrical percolation threshold of carbon black in a polymer matrix and its application to antistatic fibre, *Sci. Rep.* 9 (1) (2019) 1–12.
- [27] Alexander James Marsden, D.G. Papageorgiou, Cristina Valles, A. Liscio, V. Palermo, M.A. Bissett, R.J. Young, I.A. Kinloch, Electrical percolation in graphene-polymer composites, *2D Mater.* 5 (3) (2018) 032003.
- [28] Mathew D. Penrose, On a continuum percolation model, *Adv. Appl. Probab.* 23 (3) (1991) 536–556.
- [29] Jesper Lykke Jacobsen, High-precision percolation thresholds and Potts-model critical manifolds from graph polynomials, *J. Phys. A, Math. Theor.* 47 (13) (2014) 135001.
- [30] Stephan Mertens, Christopher Moore, Continuum percolation thresholds in two dimensions, *Phys. Rev. E* 86 (6) (2012) 061109.
- [31] Jiantong Li, Mikael Östling, Percolation thresholds of two-dimensional continuum systems of rectangles, *Phys. Rev. E* 88 (1) (2013) 012101.
- [32] Hui Yuan, Huisu Chen, Mingqi Li, Lin Liu, Zhiyong Liu, Percolation threshold and electrical conductivity of conductive polymer composites filled with curved fibers in two-dimensional space, *Soft Matter* 19 (37) (2023) 7149–7160.
- [33] Jianjun Lin, Wulong Zhang, Huisu Chen, Rongling Zhang, Lin Liu, Effect of pore characteristic on the percolation threshold and diffusivity of porous media comprising overlapping concave-shaped pores, *Int. J. Heat Mass Transf.* 138 (2019) 1333–1345.
- [34] Mingqi Li, Huisu Chen, Jianjun Lin, Rongling Zhang, Lin Liu, Effects of the pore shape polydispersity on the percolation threshold and diffusivity of porous composites: theoretical and numerical studies, *Powder Technol.* 386 (2021) 382–393.
- [35] Mingqi Li, Longbang Qing, Huisu Chen, Wenxiang Xu, Jianjun Lin, Diffusivity of porous media considering the coupling influence of pore shape- and size-polydispersities on the percolation: theoretical and numerical studies, *Comput. Methods Appl. Mech. Eng.* 404 (2023) 115830.
- [36] Mingqi Li, Huisu Chen, Lin Liu, Jianjun Lin, Karim Ullah, Permeability of concrete considering the synergetic effect of cracks shape and size polydispersities on the percolation, *Constr. Build. Mater.* 315 (2022) 125684.
- [37] Y.-B. Yi, C.-W. Wang, A.M. Sastry, Two-dimensional vs. three-dimensional clustering and percolation in fields of overlapping ellipsoids, *J. Electrochem. Soc.* 151 (8) (2004) A1292.
- [38] Heny Pratiwi, Agus Perdana Windarto, S. Susliansyah, Ririn Restu Aria, Susi Susilowati, Luci Kanti Rahayu, Yuni Fitriani, Agustiena Merdekawati, Indra Riyana Rahadjeng, Sigmoid activation function in selecting the best model of artificial neural networks, *J. Phys. Conf. Ser.* 1471 (2020) 012010.
- [39] Ahmed El Aferni, Moez Guettari, Tahar Tajouri, Mathematical model of Boltzmann's sigmoidal equation applicable to the spreading of the coronavirus (covid-19) waves, *Environ. Sci. Pollut. Res.* 28 (30) (2021) 40400–40408.
- [40] L. Haanstra, P. Doelman, J.H. Voshaar, The use of sigmoidal dose response curves in soil ecotoxicological research, *Plant Soil* 84 (2) (1985) 293–297.
- [41] Xiaotian Wu, Hao Zhang, Jun Li, An analytical approach of one-compartmental pharmacokinetic models with sigmoidal hill elimination, *Bull. Math. Biol.* 84 (10) (2022) 1–26.
- [42] Antonio Di Crescenzo, Paola Paraggio, Patricia Román-Román, Francisco Torres-Ruiz, Statistical analysis and first-passage-time applications of a lognormal diffusion process with multi-sigmoidal logistic mean, *Stat. Pap.* (2022) 1–48.
- [43] G.H.A.J.J. Kumara, Kimitoshi Hayano, Keita Ogiwara, Image analysis techniques on evaluation of particle size distribution of gravel, *Int. J. Geomate* 3 (1) (2012) 290–297.
- [44] Asghar Aryanfar, Sajed Medlej, Ali Tarhini, S. Reza Damadi, William A. Goddard III, et al., 3d percolation modeling for predicting the thermal conductivity of graphene-polymer composites, *Comput. Mater. Sci.* 197 (2021) 110650.
- [45] John A. Quintanilla, Robert M. Ziff, Asymmetry in the percolation thresholds of fully penetrable disks with two different radii, *Phys. Rev. E* 76 (5) (2007) 051115.
- [46] Mark D. Rintoul, Salvatore Torquato, Precise determination of the critical threshold and exponents in a three-dimensional continuum percolation model, *J. Phys. A, Math. Gen.* 30 (16) (1997) L585.
- [47] D.F. Holcomb, M. Iwasawa, F.D.K. Roberts, Clustering of randomly placed spheres, *Biometrika* 59 (1) (1972) 207–209.
- [48] Jacques Vieillard-Baron, Phase transitions of the classical hard-ellipse system, *J. Chem. Phys.* 56 (10) (1972) 4729–4744.
- [49] W. Xia, M.F. Thorpe, Percolation properties of random ellipses, *Phys. Rev. A* 38 (5) (1988) 2650.
- [50] Y.-B. Yi, A.M. Sastry, Analytical approximation of the two-dimensional percolation threshold for fields of overlapping ellipses, *Phys. Rev. E* 66 (6) (2002) 066130.
- [51] Jiantong Li, Mikael Östling, Precise percolation thresholds of two-dimensional random systems comprising overlapping ellipses, *Phys. A, Stat. Mech. Appl.* 462 (2016) 940–950.
- [52] John W. Perram, M.S. Wertheim, Statistical mechanics of hard ellipsoids. I. Overlap algorithm and the contact function, *J. Comput. Phys.* 58 (3) (1985) 409–416.
- [53] Wenping Wang, Jiaye Wang, Myung-Soo Kim, An algebraic condition for the separation of two ellipsoids, *Comput. Aided Geom. Des.* 18 (6) (2001) 531–539.
- [54] Salvatore Alfano, Meredith L. Greer, Determining if two solid ellipsoids intersect, *J. Guid. Control Dyn.* 26 (1) (2003) 106–110.
- [55] Dietrich Stauffer, Amnon Aharony, Introduction to Percolation Theory, Taylor & Francis, 2018.
- [56] Wenxiang Xu, Zhigang Zhu, Yaqing Jiang, Yang Jiao, Continuum percolation of congruent overlapping polyhedral particles: finite-size-scaling analysis and renormalization-group method, *Phys. Rev. E* 99 (3) (2019) 032107.
- [57] Sang Bub Lee, S. Torquato, Monte Carlo study of correlated continuum percolation: universality and percolation thresholds, *Phys. Rev. A* 41 (10) (1990) 5338.
- [58] Wenxiang Xu, Xianglong Su, Yang Jiao, Continuum percolation of congruent overlapping spherocylinders, *Phys. Rev. E* 94 (3) (2016) 032122.
- [59] Jianjun Lin, Huisu Chen, Lin Liu, Impact of polydispersity of particle shape and size on percolation threshold of 3d particulate media composed of penetrable superellipsoids, *Powder Technol.* 360 (2020) 944–955.
- [60] E.J. Garboczi, K.A. Snyder, J.F. Douglas, M.F. Thorpe, Geometrical percolation threshold of overlapping ellipsoids, *Phys. Rev. E* 52 (1) (1995) 819.
- [61] Y.-B. Yi, A.M. Sastry, Analytical approximation of the percolation threshold for overlapping ellipsoids of revolution, *Proc. R. Soc. Lond., Ser. A, Math. Phys. Eng. Sci.* 460 (2048) (2004) 2353–2380.
- [62] Abel Álvarez-Álvarez, I. Balberg, José Paulino Fernández-Álvarez, Invariant percolation properties in some continuum systems, *Phys. Rev. B* 104 (18) (2021) 184205.